Title

Strong ground motion characteristics of 2016 central italy earthquakes and implications for ground motion modeling

ISBN

9780367143282

Authors

Zimmaro, P
Stewart, JP
Scasserra, G
et al.

Publication Date

2019

Peer reviewed

Earthquake Geotechnical Engineering for Protection and Development of Environment and Constructions – Silvestri & Moraci (Eds)
© 2019 Associazione Geotecnica Italiana, Rome, Italy, ISBN 978-0-367-14328-2

Strong ground motion characteristics of 2016 Central Italy earthquakes and implications for ground motion modeling

P. Zimmaro & J.P. Stewart
University of California, Los Angeles, USA

G. Scasserra
Università degli studi del Molise, Campobasso, Italy

T. Kishida
Khalifa University of Science and Technology, Abu Dhabi, UAE

G. Tropeano
Università di Cagliari, Cagliari, Italy

ABSTRACT: The 2016 Central Italy earthquake sequence produced three mainshocks: (1) **M**6.1 24 August, (2) **M**5.9 26 October, and (3) **M**6.5 30 October. Each mainshock was followed by many aftershocks, some of which with **M** > 5.0. All earthquake events occurred on southeast-northwest trending normal faults. As part of reconnaissance activities of these events performed by the Geotechnical Extreme Events Reconnaissance Association (GEER), ground motion data was processed and analyzed. After processing all data using procedures developed during the latest Next Generation Attenuation (NGA-West2) project, we analyze strong motion characteristics of all three mainshocks, two selected large aftershocks (**M**5.3 24 August and **M**4.8 26 August) and a foreshock (**M**5.4 26 October). Our analysis shows that stations near the hanging wall, exhibit fling-step in some cases but no obvious rupture directivity effects. We compare ground motion intensity measures (including peak ground acceleration and velocity, PGA and PGV, respectively) to Italy-specific and global ground motion models. Overall, the data exhibit fast attenuation at large distance (>100 km), which is captured by Italy-adjusted global models, but not by Italy-specific models. We also found that global models tend to over-predict ground motions at short periods. Both features were also observed from the 2009 L'Aquila earthquake data and may represent regional features. We estimate the spatial distribution of PGA for the three mainshocks by means of a Kriging analysis performed on within-event residuals using a global semi-variogram model. We found that the ground motion is most intense south-west of the Mt.Vettore - Mt.Bove normal fault. Given the importance of Italian normal fault earthquakes in worldwide ground motion databases, this data set is of global significance for studies of normal fault ground motions.

1 INTRODUCTION

We analyze strong ground motion characteristics of three mainshocks, two aftershocks, and a foreshock recorded during the 2016 Central Italy earthquake sequence between 24 August and 30 October (Table 1). Our analysis is based on recordings obtained from the ESM database (Luzi et al., 2016; http://esm.mi.ingv.it). This paper summarizes main findings presented in reports by the Geotechnical Extreme Events Reconnaissance (GEER) association (GEER 2016, 2017) and Zimmaro et al. (2018). Recordings from normal faults events in Italy have a strong global significance. As shown by Zimmaro et al. (2018), in the NGA-West2 global

Table 1. Attributes of the six earthquake events analyzed.

Event date	M[1]	Number of recordings	Aftershock flag[2]	Description
24 August 2016	6.1	235	CL1	Mainshock
24 August 2016	5.3	180	CL2	Aftershock
26 August 2016	4.8	132	CL2	Aftershock
26 October 2016	5.4	178	CL1	Foreshock
26 October 2016	5.9	224	CL1	Mainshock
30 October 2016	6.5	212	CL1	Mainshock

1 Moment magnitude values from Galadini et al. (2018) and ESM database (Luzi et al., 2016).
2 CL1 = mainshocks or foreshocks, CL2 = aftershocks (Wooddell and Abrahamson, 2014).

ground motion database (Ancheta et al. 2014), 64% of normal fault recordings with **M**>5.5 are from Italian events.

We designate events as foreshocks/mainshocks (CL1), or aftershocks (CL2), using two methods: (1) the traditional approach based on time and distance windows by Gardner and Knopoff 1974, and (2) a more modern approach used in the NGA-West2 project (Bozorgnia et al. 2014) that considers the Gardner-Knopoff time window in combination with a between-event distance metric CR_{JB}, defined as the distance from the centroid of the surface projection of the possible aftershock rupture surface to the surface projection of the mainshock rupture plane (Wooddell and Abrahamson 2014). Both approaches produced similar results (Table 1).

The 2016 Central Italy earthquake sequence occurred in a gap between two damaging events: (1) the **M**6.1 1997 Umbria-Marche earthquake, and (2) the **M**6.1 2009 L'Aquila event. Figure 1 shows epicenters and finite fault models for these events, along with those for the three mainshocks recorded during the 2016 sequence. Also shown in Figure 1 are aftershocks recorded within 24 hours from each mainshock for the 24 August, 26 October, and 30 October events, along with those following a **M**5.3 event recorded on 18 January 2017 in the area of Campotosto (SE of Amatrice and NW of L'Aquila). The aftershocks for the **M**6.5 30 October event follow an expected pattern. Most epicenters are located within the surface projection of the rupture. Interestingly, this is not the case for the **M**6.1 24 August and **M**5.9 26 October events. For these two events, most of the aftershock epicenters are located outside the surface projection of the rupture (mostly south and west of the rupture).

We utilize the ground motion database presented by Zimmaro et al. (2018). All records in our database have been processed using Pacific Earthquake Engineering Research (PEER) center procedures (Ancheta et al. 2014). The database contains recordings from 298 stations. We use the time-averaged shear wave velocity (V_{S30}) as the primary site parameter. In this study, V_{S30} values were assigned to station sites using measured profiles where available, correlations based on surface geology, or the average value of the subsoil category from the Italian Building Code (Ministry of the Infrastructures 2008, NTC08) as indicated in the ESM database. Details on the adopted V_{S30} assignment protocols are provided by Scasserra et al. (2009a).

2 NEAR SOURCE GROUND MOTIONS

In this section we analyze recordings in the epicentral area of the three mainshocks of the 2016 Central Italy earthquake sequence. Clear short-duration pulses occurring early in the velocity ground motion time series are characteristics of forward directivity or fling-step effects. Recordings presented in this section were processed using special procedures to identify pulse-like features and to preserve static offsets. We first identify pulses in velocity time series using data from the mainshock with the highest magnitude (i.e. the **M**6.5 30 October event) from three stations on the hanging wall T1214, CLO, and CNE. Our analysis is based on the Shahi and Baker (2014) multicomponent pulse identification procedure. We apply this procedure

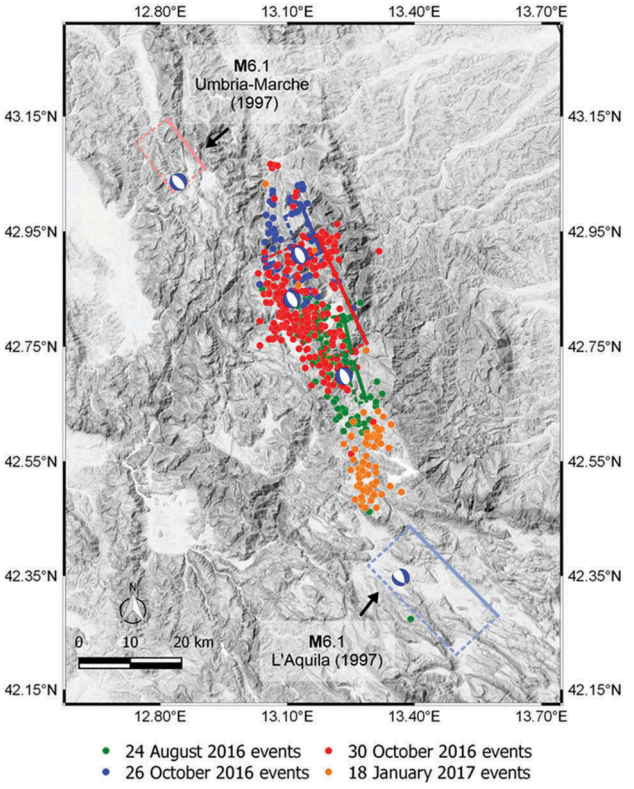

Figure 1. Map of Central Italy showing epicenters, moment tensors, and finite fault models for the following earthquakes: **M**6.1 1997 Umbria-Marche, **M**6.1 2009 L'Aquila, **M**6.1 24 August, **M**5.9 26 October, and **M**6.5 30 October. Also shown are aftershocks with **M**>3 following each mainshock of the 2016 Central Italy earthquake sequence and the 18 January 2017 event. Finite fault models from Chiaraluce et al. (2004; 1997 Umbria-Marche event), Piatanesi and Cirella (2009; 2009 L'Aquila event), Galadini et al. (2018; 2016 events).

calculating the pulse indicator for all orientations (Figure 2). We then also extract pulses and residual time series for the orientation in which velocity pulses are strongest (Figure 3). Figures 2 and 3 show that for the T1214 and CLO stations, weak pulses are present roughly in the FP orientation, while for the CNE station the algorithm does not detect significant pulses. This outcome suggests a lack of rupture directivity effects.

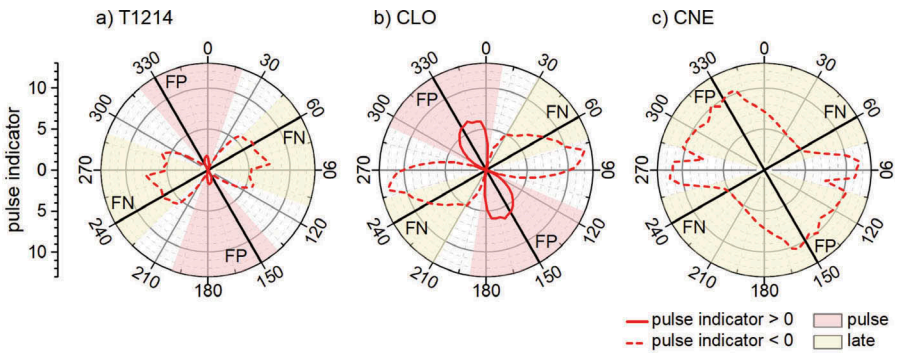

Figure 2. Pulse indicators calculated for all orientations using the Shahi and Baker (2014) identification procedure for the following stations: (a) T1214, (b) CLO, and (c) CNE.

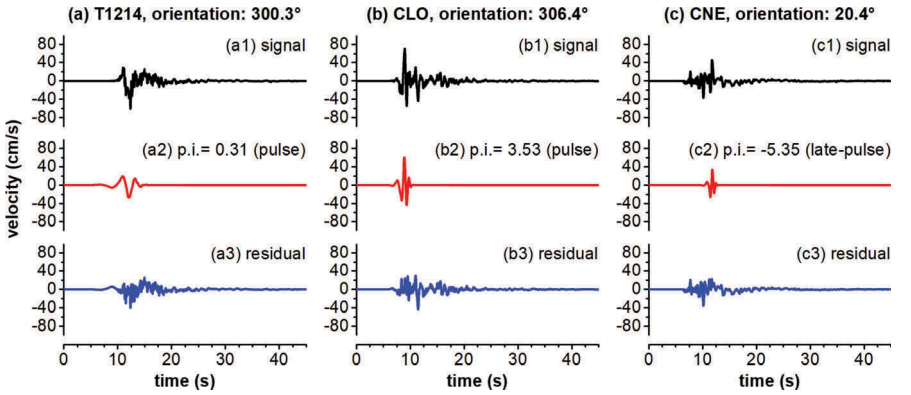

Figure 3. Original time series, extracted pulses (p.i. = pulse indicator), and residual time series for the orientation with the highest pulse indicators using the Shahi and Baker (2014) identification procedure for the following stations: (a) T1214, (b) CLO, and (c) CNE.

Another way to examine near-fault effects is to evaluate the presence of polarization of shaking in the fault normal (FN) direction at long spectral periods (e.g., Somerville et al. 1997). Zimmaro et al. (2018) show that recordings from this earthquake sequence do not show strong evidence of polarization of the ground motion in the FN direction as would be anticipated if significant forward rupture directivity effects had occurred. Our analyses indicate that forward rupture directivity effects are not significant in the ground motion recordings from these events.

Another characteristic of near-fault recordings is the presence of fling-step effects (i.e. static ground displacements, resulting from fault rupture; Kamai et al. 2014), especially on the hanging wall of dip-slip ruptures. We did not find significant fling-step effects in the near-fault records of the 24 August event (GEER 2016). We analyze the possible presence of such effects on recordings from the T1214, CLO, and CNE stations for the 30 October event. All three stations are located on the hanging wall of the fault. We reprocessed recordings from these stations using a procedure developed to preserve static displacements (Gregor et al. 2002). As shown in Figure 4, the amounts of vertical-component fling-step in records from the T1214, CLO, and CNE stations are −46 cm, −87 cm, and −16 cm, respectively. The ARQT Global

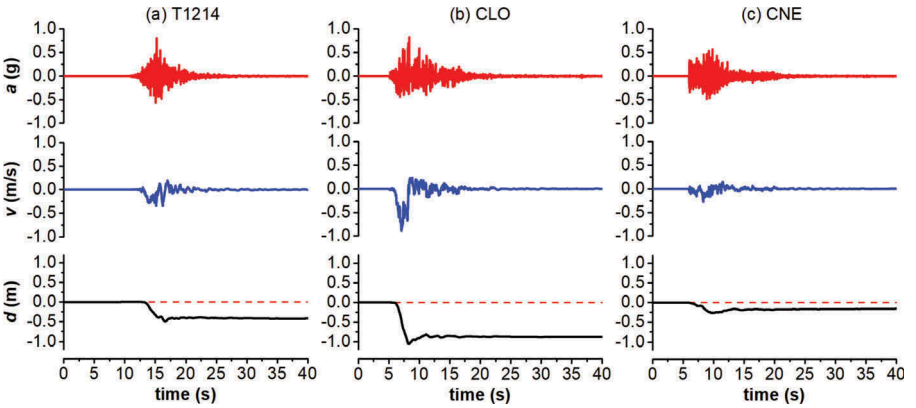

Figure 4. Vertical components of acceleration, *a*; velocity, *v*; and displacement, *d*, time series recorded at the (a) T1214, (b) CLO, and (c) CNE stations during the **M**6.5 30 October mainshock. All records were processed using the Gregor et al. (2002) procedure (from Zimmaro et al. 2018).

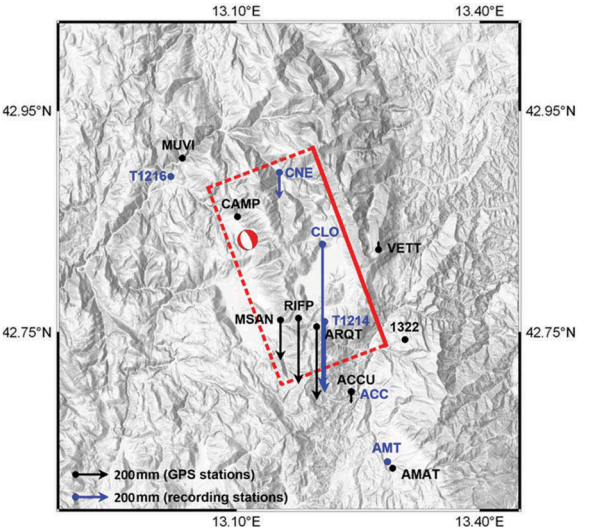

Figure 5. Vertical displacements measured during the 30 October event at strong motion recording stations (blue arrows) and GPS stations (black arrows) in the near-source area.GPS data used to produce the figure were obtained from: ftp://gpsfree.gm.ingv.it/amatrice2016/static/Cosimico_30Oct2016_GPS_GdL_V1.dat.

Positioning System (GPS) station, close to the T1214 station, recorded a vertical displacement of −45 cm. This recording is comparable to that obtained by double integration at the T1214 station (Figure 4). Other three ground motion stations ACC, AMT, and T1216 (not on hanging wall) have nearly co-located GPS stations (ACCU, AMAT, and MUVI, respectively). Figure 5 shows a map that compares vertical displacements measured at GPS and strong motion stations in the epicentral area of the 30 October event. All pairs of co-located GPS and strong motion stations provide comparable values of vertical displacements. These results are in good agreement with similar analyses performed by Luzi et al. (2017) and D'Amico et al. (2019).

3 COMPARISON WITH GROUND MOTION MODELS AND RESIDUALS ANALYSIS

Recently, several studies focused on the selection of suitable ground motion models (GMMs) for use in global (Stewart et al. 2015), regional (Delavaud et al. 2012), or site-specific applications in Italy (Zimmaro and Stewart 2017). Local models (i.e. calibrated on local ground motion databases) can reflect local geologic and tectonic conditions, which may differ from those represented by global models. However, the limited database size used to develop local models may be inadequate to constrain GMMs for conditions often critical for application (e.g. large magnitudes and small distances). Global models are more effective for such conditions, because they are typically based on much larger worldwide databases but may contain bias with respect to local effects. Regional adjustment factors can be used to reduce the bias of global models. Such factors are typically applied to anelastic attenuation and site effect components of the GMMs.

In this section we compare recorded data to the following GMMs applicable to shallow-crustal earthquakes in active tectonic regions: (1) an Italy-specific model by Bindi et al. (2011; hereafter Bea11), (2) the average of three NGA-West2 GMMs, without regional adjustments (Boore et al. 2014, Campbell and Bozorgnia 2014, Chiou and Youngs 2014; hereafter NGA2), and (3) the average of those same three NGA-West2 models but now applying regional adjustments for Italy (NGA2-I). All distances are calculated using the trimmed finite-fault models for the three mainshocks (Galadini et al. 2018). We idealize aftershocks and foreshocks (**M**4.8-5.4) as point sources for calculating distances.

Figures 6 and 7 show the distance dependence of median-component peak acceleration (PGA) and velocity (PGV) for the six events in Table 1, along with predictions from the Bea11 model, the average of the NGA2 models, and the average of the NGA2-I models. Median predictions have been calculated using V_{S30} = 580 m/s (considered representative of site conditions in the area). Recorded data are plotted with different symbols for three site categories (categories A, B, and C, respectively according to NTC08): (1) rock (V_{S30} > 800 m/s), (2) stiff soil and weathered rock (360 < V_{S30} < 800 m/s), and (3) soft soil (V_{S30} < 360 m/s). All three GMMs fit the data reasonably well for R_{JB} in the range 0 - 100 km. Beyond 100 km,

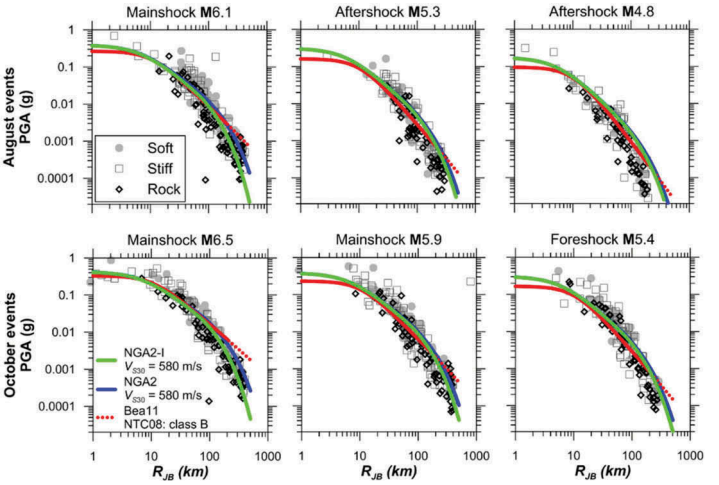

Figure 6. Variation of PGA with R_{JB} for rock (NTC08: A), stiff soil (NTC08: B), and soft soil (NTC08: C, D, E) and predictions from the selected ground motion models. For Bea11 (red lines), dotted lines indicate predictions beyond the published range of model validity (from Zimmaro et al. 2018).

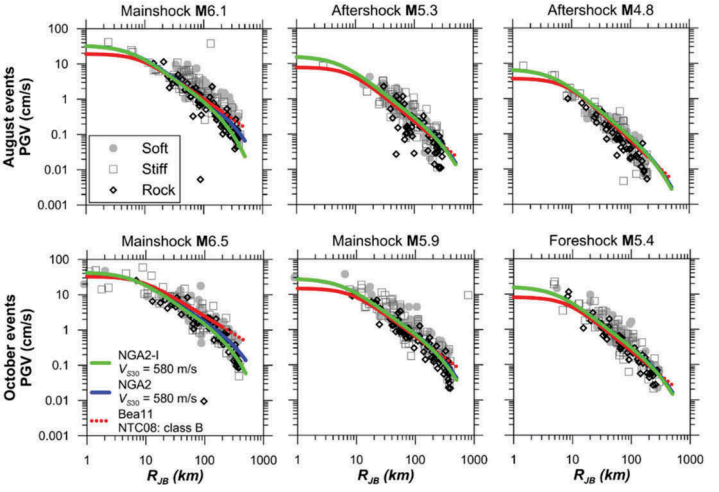

Figure 7. Variation of PGV with R_{JB} for rock (NTC08: A), stiff soil (NTC08: B), and soft soil (NTC08: C, D, E) and predictions from the selected ground motion models. For Bea11 (red lines), dotted lines indicate predictions beyond the published range of model validity (from Zimmaro et al. 2018).

there is a relatively fast attenuation of ground motions in all six events. This feature, captured by the NGA2-I models (with regional adjustment for Italy), is a characteristic of Italian data observed from pre-2006 data by Scasserra et al. (2009b) and from the L'Aquila event sequence by Stewart et al. (2012). This effect seems to be persistent in Italian data. Similar trends of fast anelastic attenuation with distance have been observed in data from Japan (e.g. Boore et al. 2014). This effect seems to be related to low values of the seismic quality factor (Q). At short distances (i.e. 1 - 10 km), data are sparse, but there are differences among models. In particular, Bea11 has a wider flat-attenuation region at close distance, likely due to the use of a larger near-source saturation term.

We further analyze the comparison between recorded data and prediction using residual analysis. We calculate total residuals for each data point as follows:

$$R_i = \ln(Y_i) - \mu_{ln}(\mathbf{M},\ R_i,\ V_{S30,i}) \tag{1}$$

where Y_i is the ground motion intensity measure from recording i and μ_{ln} is the natural log mean for that same intensity measure from a GMM, with the appropriate arguments for the model (magnitude **M**, distance R, site parameter V_{S30}). For the NGA-West2 models (NGA2 and NGA2-I), μ_{ln} is taken as the average of the natural log means of the three considered GMMs. For Bea11, the median prediction is used. Total residuals are then partitioned as follows to compute the random effect for each event η (also called the event term), and the remaining residual ε (also called within-event residual) (e.g., Stafford, 2012):

$$R_i = c_k + \eta + \varepsilon_i \tag{2}$$

where c_k is a bias term assumed for the present analysis to be null (to the extent that such a bias might exist, it is included in our estimates of η).

Figures 8 and 9 show within-event residuals for PGA and PGV for all six events as a function of distance. Binned means and standard deviations are shown using five bins per log-cycle (due to limited data, a single bin is used for R_{JB} = 0 - 10 km). The analysis of Figures 8 and 9 indicates that there is good consistency between GMMs and mainshock data up to 100 km. At large distance (R_{JB} > 100 km), the Bea11 residuals consistently trend downwards, indicating underprediction of anelastic attenuation in this model. For the NGA2 and NGA2-I models, the residuals trends upwards for some events and downwards for others, indicating that the anelastic attenuation is somewhat variable between events but may be reasonable in an average sense. The recommended distance range for the Bea11 model is 0 - 200 km. As a result, residuals for distances beyond 200 km represent model extrapolations. Further discussions of GMM-data comparisons and residuals analysis are provided by Zimmaro et al. (2018).

Figure 10 shows the event terms as a function of oscillator period for the six analyzed earthquakes. Also shown are plus/minus one between-event standard deviations from the Boore et al. (2014) and the Bindi et al. (2011) GMMs. For short periods (PGA to 0.5 s), the Central Italy event terms for the NGA2-I range from zero to -1, whereas they are nearly zero for longer periods. This trend is consistent with what was observed for the 2009 L'Aquila event ground motions using earlier versions of NGA models (i.e. NGA-West1 GMMs) with an Italy-specific adjustment (Stewart et al., 2012).

The bulk of this study has been performed as part of the GEER-led post-earthquake reconnaissance effort following the 24 August and October 2016 events. As such, we estimated the spatial distribution of ground shaking to better examine the effects of this earthquake sequence on the natural and built environment. We performed Kriging of within-event residuals, ε, for the three mainshocks using the NGA2-I GMMs and the global semi-variogram model by Jayaram and Baker (2009). We then computed ground motion intensity measures for location j as:

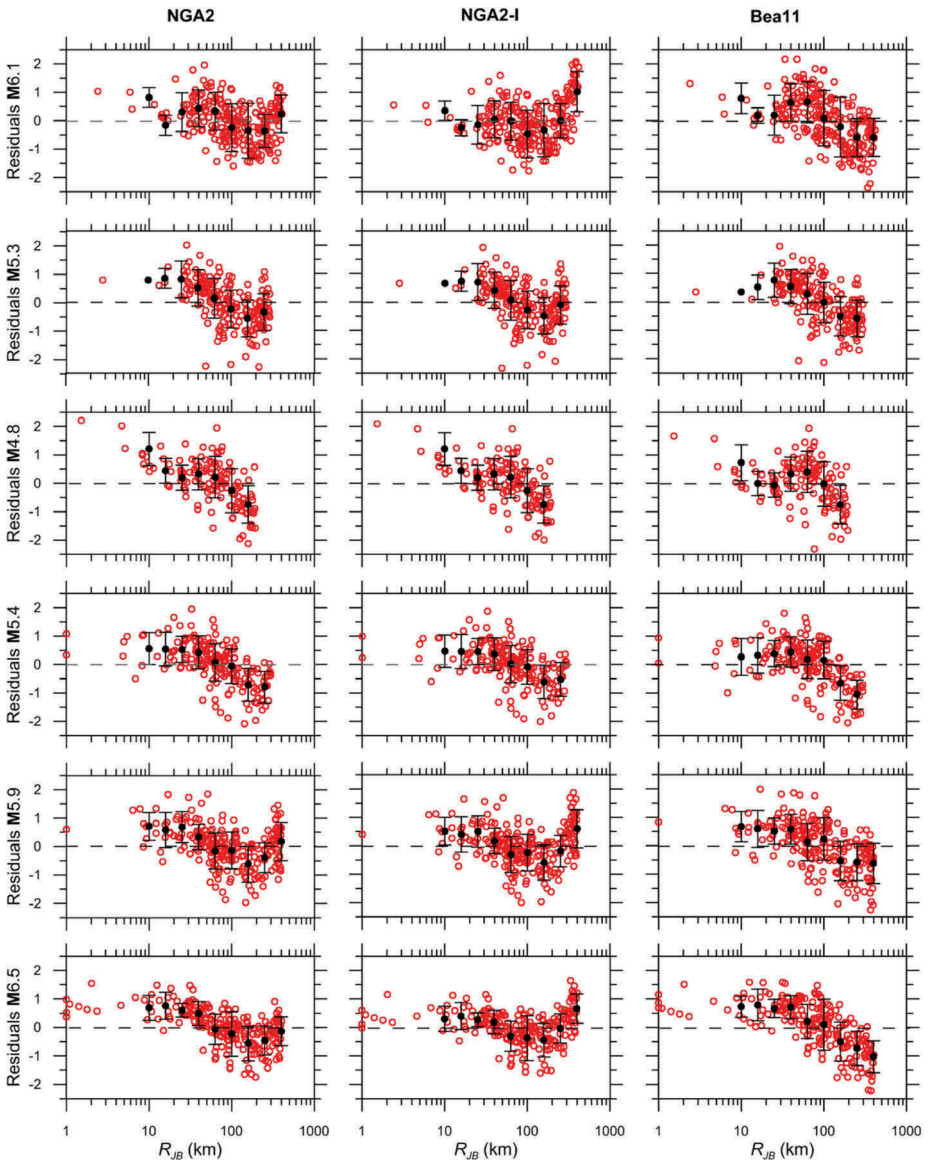

Figure 8. Within-event residuals of PGA from recorded ground motions relative to predictions of the NGA2, NGA2-I, and Bea11 GMMs. Binned means shown with ± one standard deviation. (from Zimmaro et al. 2018).

$$\overline{\ln(Y)}_j = \mu_{ln}(\mathbf{M},\ R_j,\ V_{S30,j}) + \eta + \varepsilon_j \tag{3}$$

where $\overline{\ln(Y)}_j$ is the mean estimate of the ground motion intensity measure for location j. As in Eq. (1), the natural log mean on the right side is taken as the average of the means from the NGA2-I models. Figure 11 shows a map of the spatial distribution of PGA for the **M**6.1 24 August, **M**5.9 26 October, and **M**6.5 30 October mainshocks. These maps are prepared for a uniform site condition of V_{S30} = 580 m/s. The **M**6.1 24 August event is a

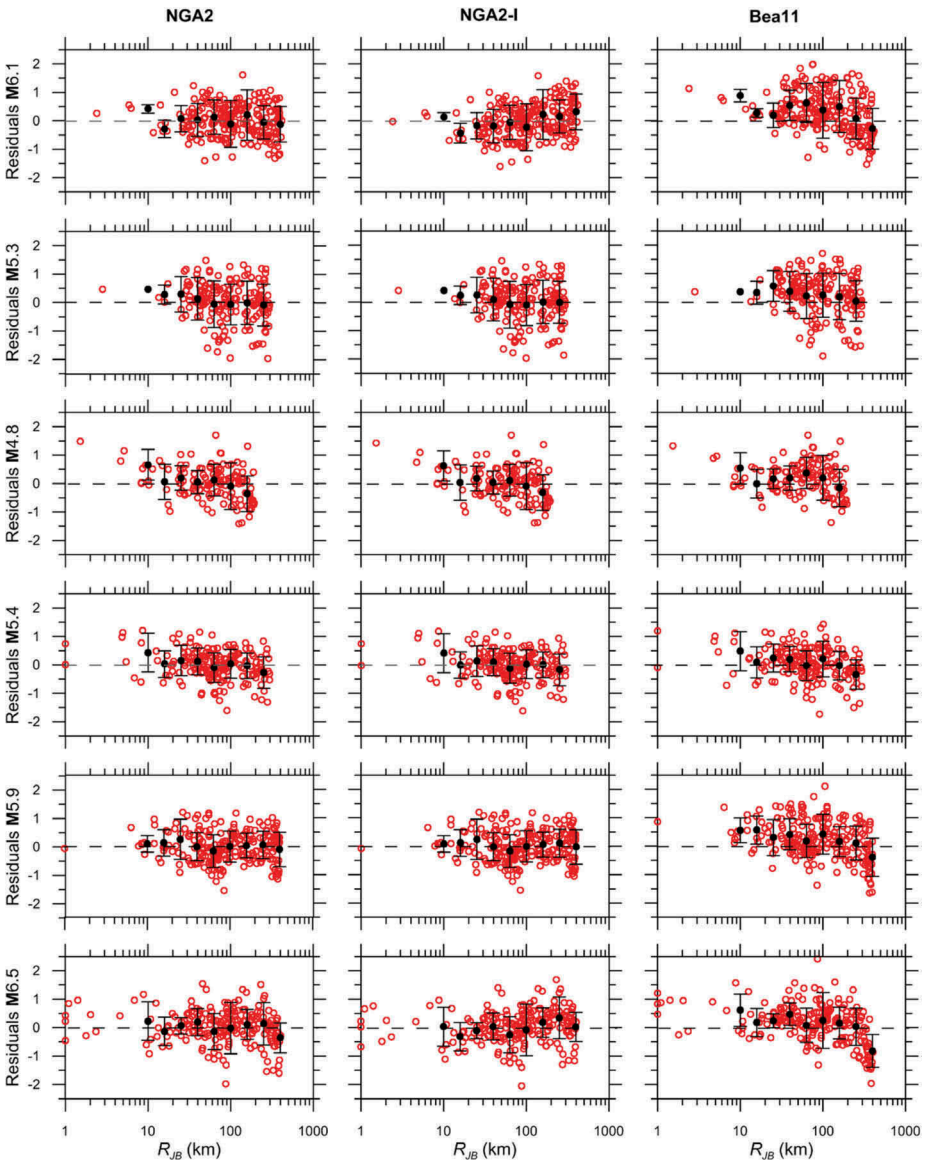

Figure 9. Within-event residuals of PGV from recorded ground motions relative to predictions of the NGA2, NGA2-I, and Bea11 GMMs. Binned means shown with ± one standard deviation. (from Zimmaro et al. 2018).

two-segment rupture (Galadini et al., 2018). For this event the highest ground motion intensities are localized in the proximity of the southern segment (Amatrice fault). For the 26 and 30 October events, the highest values of PGA are located in the south-western portion of the finite fault models.

The ground motions in these maps do not account for local site response effects (topographic effects) that appears to be significant in several damaged regions (Sextos et al., 2018). Additional results, including maps of spatial distribution of within-event residuals for all three mainshocks are provided by GEER (2017) and Zimmaro et al. (2018).

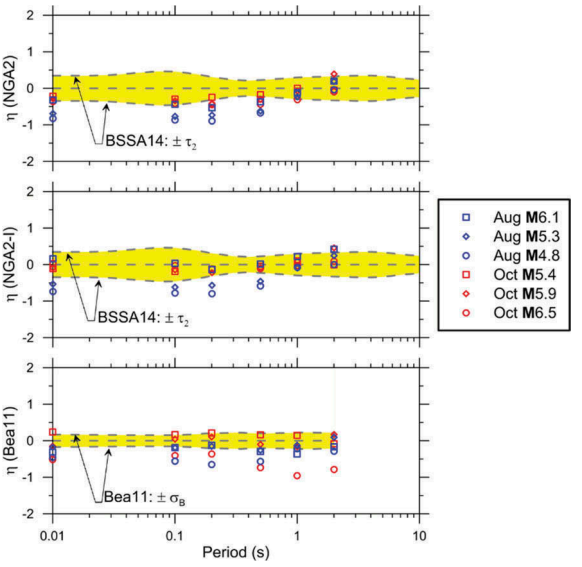

Figure 10. Event terms for PGA and PSA oscillator periods of 0.1 - 2.0 s for the three sets of models and six events. For context, the ± one between-event standard deviation is shown: τ_2 for **M**>5.5 from the Boore et al (2014) and σ_B from Bindi et al (2011).

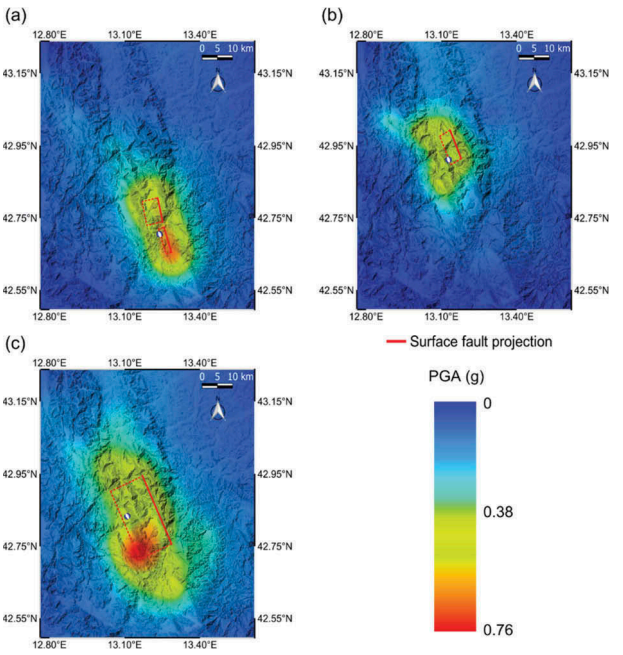

Figure 11. Spatial distribution of PGA for the (a) 24 August, (b) 26 October, and (c) 30 October earthquake.

4 CONCLUSION

We perform a comprehensive characterization of strong ground motions recorded during the 2016 Central Italy earthquake sequence. This paper is based on analysis performed as part of GEER post-earthquake reconnaissance missions (GEER 2016, 2017, Zimmaro et al. 2018).

We use special processing techniques to preserve fling-step effects. We identify various cases in the near-source area for which displacements observed at strong motion stations during the 30 October mainshock are similar to those from adjacent GPS sensors. We also examined the available ground motion data for evidence of rupture directivity, but found neither consistent polarization of ground motion in the fault normal direction nor clear evidence of pulse-like features in velocity time series.

We analyze recorded data relative to local and global GMMs. We found that data from this earthquake sequence show a relatively fast anelastic attenuation with distance for $R_{JB} > 100$ km. This feature is captured to a mixed degree by available models. These effects were already observed in data from Italian dip-slip earthquakes and should be incorporated into future Italy-specific models.

We produce maps showing the spatial distribution of selected intensity measures. We show that PGA values during the 24 August event are higher in the area of the Amatrice fault. For the 26 and 30 October mainshocks, the highest values of PGA are located in the south-western portion of the finite fault models.

ACKNOWLEDGEMENTS

The GEER Association is supported by the National Science Foundation (NSF) through the Geotechnical Engineering Program under Grant No. CMMI-1266418. Any opinions, findings, and conclusions or recommendations expressed in this material are those of the authors and do not necessarily reflect the views of the NSF. The GEER Association is made possible by the vision and support of the NSF Geotechnical Engineering Program Directors: Dr. Richard Fragaszy and the late Dr. Cliff Astill. GEER members also donate their time, talent, and resources to collect time-sensitive field observations of the effects of extreme events.

REFERENCES

Ancheta, T.D. and other 11 authors, 2014. NGA-West2 database. *Earthq. Spectra*, 30, 989–1005.

Bindi, D., Pacor, F., Luzi, L., Puglia, R., Massa, M., Ameri, G., Paolucci, R., 2011. Ground motion prediction equations derived from the Italian strong motion database. *Bull. Earth. Eng*., 9, 1899–1920.

Boore, D. M., Stewart, J.P., Seyhan, E., Atkinson, G.M., 2014. NGA-West 2 equations for predicting PGA, PGV, and 5%-damped PSA for shallow crustal earthquakes. *Earthq. Spectra*, 30, 1057–1085.

Bozorgnia, Y. and other 31 authors, 2014. NGA-West 2 research project. *Earthq. Spectra*, 30, 973–987.

Campbell, K.W. & Bozorgnia, Y., 2014. NGA-West2 ground motion model for the average horizontal components of PGA, PGV, and 5% damped linear acceleration response spectra. *Earthq. Spectra*, 30, 1087–1115.

Chiaraluce L., Amato, A., Cocco, M., Chiarabba, C., Selvaggi, G., Di Bona, M., Piccinini, D., Deschamps, A., Margheriti, L., Courboulex, F., Ripepe, M., 2004. Complex Normal Faulting in the Apennines Thrust-and-Fold Belt: The 1997 Seismic Sequence in Central Italy. *Bull. Seism. Soc. Am*., 94, 99–116.

Chiou, B.S.J. & Youngs, R.R., 2014. Update of the Chiou and Youngs NGA model for the average horizontal component of peak ground motion and response spectra. *Earthq. Spectra*, 30, 1117–1153.

D'Amico, M., Felicetta, C., Schiappapietra, E., Pacor, F., Gallovic, F., Paolucci, P., Puglia, R., Lanzano, G., Sgobba, S., Luzi L., 2019. Fling effects from near-source strong-motion records: insights from the 2016 M_w6.5 Norcia, Central Italy, earthquake. *Seismol. Res. Lett*., 90, 659–671.

Delavaud, E., Cotton, F., Akkar, S., Scherbaum, F., Danciu, L., Beauval, C., Drouet, S., Douglas, J., Basili, R., Sandikkaya, M.A., Segou, M., Faccioli, E., Theodoulidis, N., 2012. Toward a ground-motion logic tree for probabilistic seismic hazard assessment in Europe. *Journal of Seismology*, 16, 451–473.

Galadini F., Falcucci E., Gori S., Zimmaro P., Cheloni D., Stewart J.P., 2018. Active Faulting in Source Region of 2016–2017 Central Italy Event Sequence. *Earthq. Spectra*, 34, 1557–1583

Gardner, J.K. & Knopoff, L., 1974. Sequence of earthquakes in Southern-California, with aftershocks removed, Poissonian? *Bull. Seism. Soc. Am*., 64, 1363–1367.

GEER, 2016. Engineering reconnaissance of the 24 August 2016 Central Italy Earthquake. Version 2, Zimmaro, P. and Stewart, J. P. (editors), Geotechnical Extreme Events Reconnaissance Association Report No. GEER-050B. doi: 10.18118/G61S3Z.

GEER, 2017. Engineering reconnaissance following the October 2016 Central Italy Earthquakes - Version 2, Zimmaro, P. and Stewart, J. P. (editors), Geotechnical Extreme Events Reconnaissance Association Report No. GEER-050D. doi: 10.18118/G6HS39.

Gregor, N., Silva, W.J., Darragh R.B., 2002. Development of attenuation relations for peak particle velocity and displacement. A PEARL report to PG&E/CEC/Caltrans, June 12, 2002.

Jayaram, N. & Baker, J.W., 2009. Correlation model for spatially distributed ground-motion intensities, *Earthquake Engineering and Structural Dynamics*, 38, 1687–1708.

Kamai, R., Abrahamson, N.A., Graves, R.W. 2014. Adding fling effects to processed ground-motion time histories, *Bull. Seism. Soc. Am*., 104, 1914–1929.

Luzi, L., Pacor, F., Puglia, R., Lanzano, G., Felicetta, C., D'Amico, M., Michelini, A., Faenza, L., Lauciani, V., Iervolino, I., Baltzopoulos, G., Chioccarelli, E., 2017. The Central Italy seismic sequence between August and December 2016: analysis of strong-motion observations. *Seismol. Res. Lett*., 88, 1219–1231.

Luzi, L., Puglia, R., Russo, E., ORFEUS WG5, 2016. Engineering strong motion database, version 1.0. Istituto Nazionale di Geofisica e Vulcanologia, Observatories & Research Facilities for European Seismology. doi: 10.13127/ESM.

Ministry of the Infrastructures - Italy, 2008. Norme tecniche per le costruzioni, Decree of the Minister of the Infrastructures, 14 January 2008, Gazzetta Ufficiale della Repubblica Italiana No. 29, Rome, Italy.

Piatanesi A. & Cirella A., 2009. Rupture Process of the 2009 Mw6.3 L'Aquila (Central Italy) Earthquake from Nonlinear Inversion of Strong Motion and GPS Data. Istituto Nazionale di Geofisica e Vulcanologia (INGV), Rome, Italy.

Scasserra G., Stewart J.P., Kayen R.E., Lanzo G., 2009a. Database for earthquake strong motion studies in Italy. *Journal of Earthquake Engineering*, 13, 852–881.

Scasserra, G, Stewart, J.P., Bazzurro, P., Lanzo, G., Mollaioli, F., 2009b. A comparison of NGA ground-motion prediction equations to Italian data. *Bull. Seism. Soc. Am*., 99, 2961–2978.

Sextos A. and other 18 authors, 2018. Local site effects and incremental damage of buildings during the 2016 Central Italy earthquake sequence. *Earthq. Spectra*, 34, 1639–1669.

Shahi, S.K. & Baker, J.W., 2014. An efficient algorithm to identify strong-velocity pulses in multicomponent ground motions. Bull. Seism. Soc. Am., 104, 2456–2466.

Somerville, P. G., Smith, N. F., Graves, R.W., Abrahamson, N. N., 1997. Modification of empirical strong ground motion attenuation relations to include the amplitude and duration effects of rupture directivity, *Seismol. Res. Lett*., 68, 199–222.

Stafford, P.J., 2012. Evaluation of structural performance in the immediate aftermath of an earthquake: a case study of the 2011 Christchurch earthquake, *International J. of Forensic Engineering*, 1, 58–77.

Stewart, J.P., Douglas, J., Javanbarg, M., Bozorgnia, Y., Abrahamson, N.A., Boore, D. M., Campbell, K. W., Delavaud, E., Erdik, M., Stafford, P. J., 2015. Selection of ground motion prediction equations for the Global earthquake model. *Earthq. Spectra*, 31, 19–45.

Stewart, J.P., Lanzo, G., Pagliaroli, A., Scasserra, G., Di Capua, G., Peppoloni, S., Darragh, R.B., Gregor, M., 2012. Ground Motion Recordings from the Mw 6.3 2009 L'Aquila Earthquake in Italy and their Engineering Implications. *Earthq. Spectra*, 28, 317–345.

Wooddell, K.E. & Abrahamson, N. A., 2014. Classification of main shocks and aftershocks in the NGA-West2 database. *Earthq. Spectra*, 30, 1257–1267.

Zimmaro P., Scasserra G., Stewart J.P., Kishida T., Tropeano G., Castiglia M., Pelekis P., 2018. Strong Ground Motion Characteristics from 2016 Central Italy Earthquake Sequence. *Earthq. Spectra*, 34, 1611–1637.

Zimmaro, P. & Stewart, J.P., 2017. Site-specific seismic hazard analysis for Calabrian dam site using regionally customized seismic source and ground motion models. *Soil Dynam. Earthq. Eng*., 94, 179–192.